entropy

MDPI

Article

Percolation with Distance-Dependent Site Occupational Probabilities

Eleftherios Lambrou and Panos Argyrakis *

Department of Physics and Complexity Center, University of Thessaloniki, GR-54124 Thessaloniki, Greece; lamele@pogoni.gr
* Correspondence: panos@auth.gr

Abstract

We introduce a new method for preparing a percolation system by employing an inverse percolation model. Unlike standard percolation, where the site occupancy is uniform, the new model imposes a distance-dependent probability of site removal, where sites closer to the lattice center have a higher probability of being removed and are more prone to damage as compared to those at the periphery of the system. The variation in this removal probability is a function of the distance (d) from the central point. Thus, the central point plays a key role. This is reflected in our effort to model the role of a tumor cell and its surroundings (the tumor microenvironment). The tumor causes a decrease in the concentration of key elements, such as O_2 (resulting in hypoxia) and Ca, in the region close to it, which in turn is an impediment to the efficiency of radiotherapy and chemotherapy. This decrease is the largest in sites adjacent to the tumor and smaller away from the tumor. Such change in the concentrations of these elements is vital in the mechanism of cancer therapies. Starting from a fully occupied lattice, we introduce a distance-dependent removal probability $q(d)$. The value of $q(d)$ is 1 at and next to the tumor (center) and decreases linearly away from it to a limiting value q_p, which is the value of q at the lattice boundaries. We investigate the system properties as a function of q_p and observe a significant decrease in the critical percolation threshold p_c as q_p decreases, falling from the standard value of $p_c = 0.5927$ to approximately $p_c = 0.20$. Furthermore, we demonstrate that the size of the spanning cluster and the total number of clusters exhibit a strong dependence on q_p as well.

Keywords: inverse percolation; distance-dependent occupational probability; hypoxia heterogeneity; tumor radiotherapy; Monte-Carlo simulations; oncology radiation modeling

Academic Editor: Robert M. Ziff

Received: 19 December 2025
Revised: 15 January 2026
Accepted: 20 January 2026
Published: 22 January 2026

1. Introduction and the Model

The percolation model [1] is a classical paradigm in Statistical Physics for describing a binary disordered system, and together with the Ising model its constitutes the simplest model [2] for randomly mixed systems. While by their very nature these systems are mathematical/geometrical structures, nevertheless, in the past fifty years the rapid progress in the development of new algorithms has opened the way to a large variety of applications, ranging from randomly mixed crystals [3,4] to fluid flow in porous media [5,6], gelation and polymerization [7,8], porosity and adsorption [9,10], and more recently networks [11–13], studying their robustness [14], the spreading of diseases in epidemics [15,16], the spreading of rumors and gossip on social media [17–21], the spreading of crises and innovations in economic networks [22], and a large variety of other fields not possible to

enumerate here. Recently [23,24], a crude percolation model was proposed by us to study the depletion of key chemical elements in the vicinity of cancerous tumor cells, which results in hampering the effectiveness of crucial therapies for the curing of cancer. That model presented preliminary findings on how the percolation phase transition changes with the depletion of these elements. Near and around the area of a tumor there is the so-called microenvironment (TME), an area that is strongly affected by the tumor and is characterized by a change in the normal density of constituents, producing a density gradient and degrading the results of applied therapies, such as chemotherapy and radiation. The center of mass of the tumor containing the tumor cells can then proceed more easily to metastasis, which is very precarious for the living organism. Specifically, in the TME the tumor is able to affect the oxygen content, which results in the depletion of O_2 or hypoxia [25–28], the concentration of extracellular potassium ions, leading to excess of K^+ or hyperkalemia [29–31], and its acidity, i.e., increase in H^+ or lowering of pH [32–34].

It is therefore important to explore in detail the constituents and concentration of the above species in the TME, its mass distribution, and its gradient density, as they all have important implications for understanding the tumor biology and the subsequent medical treatment. The important factor therefore is the gradient density of these constituents, as a function of distance from the center of the tumor. Thus, chemotherapy treatment may be effective only at the TME periphery and beyond because the drug cannot easily progress into the tumor center, as it may be hampered by the TME's acidity. Similarly due to hypoxia, the O_2 depletion at the center of a tumor will differ from that at its periphery. Such depletion, while always reducing the efficiency of any radiation therapy, may also affect its combination with chemotherapy. Additionally, the distribution of the TME's hyperkalemia may affect the success of immunochemistry.

In the current work we propose to study the interplay of the concentration gradient between the tumor core and the TME periphery using the percolation model. Notably, the information on the distributions of the molecular species discussed above may elucidate the importance of the different therapy options, i.e., whether radiation or chemotherapy is appropriate, or a combination therapy of these two, or even if surgery would be the most appropriate route. Imaging is also used to visualize, detect, diagnose, and monitor tumors within the body, and together with therapy its is often affected by tumor penetration difficulty, either by the drug or by the imaging contrast agent [35].

The percolation system is defined as a geometrical structure made of two components that are randomly mixed. In the case of a lattice, we consider the lattice sites as being either empty or occupied. Similarly, an analogous situation is if the bonds connecting pairs of sites exist or not. One could correspond the presence or absence of lattice sites with that of the molecular species discussed above. We use the probability p to designate if a site is occupied or not, with p being in the range $0 < p < 1$. Thus, $p = 0$ signifies a totally empty lattice, while $p = 1$ corresponds to a fully occupied lattice. Occupied sites that are adjacent (nearest neighbors) form clusters of sites. Initially the lattice is empty ($p = 0$). Sites start to become occupied when p increases, and clusters of sites are formed. The basic characteristic is that the system undergoes a sudden phase transition characterized by a sharp change in the connectivity of the system that depends entirely on the probability p. This transition is characterized by a critical value of the parameter p, which is called p_c, and it is defined as the point where for the first time a large spanning cluster is formed with occupied sites at opposite ends of the lattice. Such a transition is a second-order phase transition, and it is characterized by several properties, as indicated by a series of critical exponents that have been investigated in detail in the past [36]. In this context, the probability p acts as the control parameter of the system. The order parameter is defined as the probability $P\infty$ that a site belongs to the spanning cluster, which determines the state of the system. In the

classical percolation model, all sites are characterized by the same probability p of being occupied, uniformly distributed across the entire lattice. In the present work we define a new model in which p (the probability for a site to be occupied) is not uniform in the entire lattice but depends on the distance from a particular lattice point, with this point typically being the center of the lattice. This is done so in our effort to imitate the tumor microenvironment, for which we want a concentration gradient with respect to the central point. Our motive emanates from our effort to build a model in which a central point plays a key role in allowing neighboring sites to be occupied or not, depending on their distance from it. A real situation can be visualized in a tumor system in which the tumor itself is able to modify the concentration of key elements in its close neighborhood, such as O_2 and K^+, by reacting with them and depleting their needed concentration for the therapy to be effective in killing the tumor cells.

In the current study we start with a fully occupied lattice and then use an inverse percolation model. We start to randomly remove sites, but now instead of using the probability p, which is the same for the entire lattice, we define q as the probability that a given site will be removed from the lattice, which now depends on the distance from a certain point. We choose the center of the lattice as the "tumor cell" and we set $q = 1$ at the lattice center. The removal probability q decreases linearly with the distance from the center, reaching a boundary value denoted by the parameter q_p at the perimeter of the lattice.

2. Methodology

We start with a two-dimensional square lattice of size $L \times L$. Initially, the lattice is fully occupied ($p = 1$). Our goal is to remove sites, one by one, until we reach the critical percolation threshold, defined as the first moment when the largest connected cluster ceases to exist upon the removal of the last site. This point is commonly known as the red-bond point. In the classical site percolation (where sites are removed at random), the critical threshold is well-known, $p_c \approx 0.5927$, and is defined as the point where a connected cluster spans the lattice from one side to the opposite (top to bottom or right to left).

In this new model, a spatial bias is introduced in the site removal process. Sites are chosen at random to be inspected for possible removal. The probability of removal, q, is no longer uniform but depends on the site's distance from the center of the lattice. The model is governed by the parameter $q_p \in [0, 1]$, which represents the boundary value of the removal probability at the lattice perimeter. Specifically, the removal probability $q(d)$ is a function of the distance d from the center such that $q = 1$ at the origin and scales linearly to $q(d_{max}) = q_p$ at the boundary.

The probability of removal $q(d)$ at a site located at a distance d from the lattice center is calculated using the linear gradient

$$q(d, q_p) = 1 - (1 - q_p)\frac{d}{d_{\max}} = 1 - \frac{2(1 - q_p)}{L - 1}d \tag{1}$$

where $d_{\max} = (L - 1)/2$ is the distance from the center to the perimeter of the lattice, d is the distance from the center to the site, and q_p is the boundary parameter.

To further understand the dynamics described by Equation (1), it is instructive to analyze the extreme conditions of the function $q(d, q_p)$ and their corresponding physical meanings. In the limit where $q_p = 1$, the removal probability becomes constant across the entire lattice, $q(d, 1) = 1$ for all d, representing a scenario where the infection is so aggressive that it leads to a uniform and instantaneous removal of all sites. Conversely, the case $q_p = 0$ represents the maximum possible spatial gradient; here, removal is certain at the center ($q = 1$) but the probability vanishes at the perimeter ($q = 0$), modeling a

localized tumor where the infection's impact diminishes completely at the boundaries. Furthermore, for any value of q_p, the center of the lattice ($d = 0$) remains the primary source of the process with $q = 1$, while at the perimeter ($d = d_{\max}$), the probability is identically q_p, confirming that q_p acts as a control parameter that adjusts the intensity of the infection's spatial decay. The distance d between a point (x, y) and the center (x_c, y_c) of the square lattice can be measured in several ways, and the choice of metric may impact the geometry of the iso-probability contours. These include the following ways: (1) the maximum norm metric (L_∞), (2) the Euclidean distance (L_2 norm), and (3) the Manhattan distance (L_1 metric or taxicab geometry) [37]. For completeness we will briefly describe each one of them and schematically show their properties

(1) Maximum norm metric (L_∞)

$$d = \max(|x - x_c|, |y - y_c|) \tag{2}$$

The geometric locus of the iso-probabilities (points with the same q) forms a square.

(2) Euclidean distance (L_2 norm)

$$d = \sqrt{(x - x_c)^2 + (y - y_c)^2} \tag{3}$$

The iso-probabilities form circles.

(3) Manhattan distance (L_1 metric)

$$d = |x - x_c| + |y - y_c| \tag{4}$$

The iso-probabilities form a diamond shape (square rotated by 45 degrees).

The spatial distribution of the removal probability and the resulting geometry of the lattice are illustrated in Figure 1. This figure showcases how the choice of distance metric (L_∞, L_2, and L_1) reshapes the iso-probability contours, effectively altering the 'footprint' of the infection. In the first column (L_∞), the contours maintain a square symmetry, whereas the Euclidean metric (L_2) produces circular patterns, and the Manhattan metric (L_1) results in diamond-shaped contours. Moving from the top to the bottom rows, we observe the effect of decreasing the boundary parameter q_p. As q_p is reduced, the gradient between the center ($q = 1$) and the perimeter becomes steeper. Visually, the central lighter regions represent areas with a high probability of site removal ($q \to 1$), while the darker peripheral regions indicate a higher probability of sites remaining occupied $(1 - q) \to 1$. This visualization confirms that for lower q_p values, the 'survival probability' of the cells increases significantly as we move toward the lattice edges, effectively confining the most intense part of the removal process to the core of the structure.

The choice of metric defines the shape of the region with the same removal probability. In the current work we will use the maximum norm metric ($L\infty$ metric), although we do not expect significant differences using any of the other two ways.

The L_∞ metric was chosen as the primary focus because its square iso-probability contours align perfectly with the boundaries of the square lattice used in our simulations. This alignment allows for a more straightforward interpretation of the boundary parameter q_p and its effect on the global connectivity of the system.

By varying q_p, we effectively modulate the boundary conditions of the infection process. This parameter determines the steepness of the probability gradient between the center and the perimeter. Specifically, lower values of q_p correspond to a more pronounced spatial decay of the removal probability, thereby increasing the likelihood of site survival as we move toward the lattice boundaries.

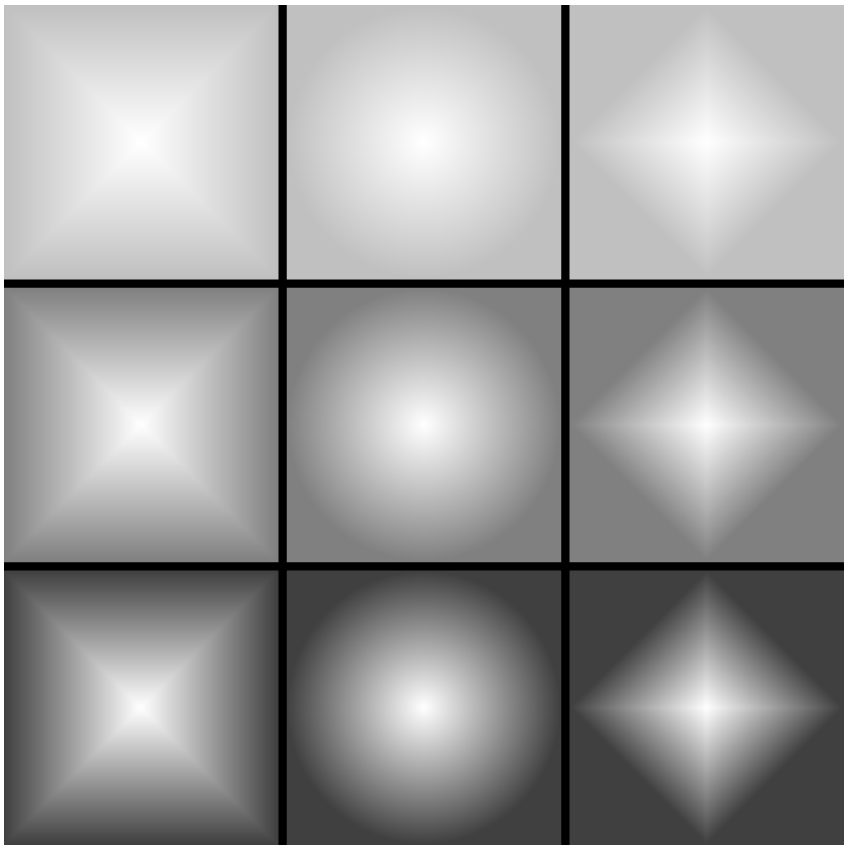

Figure 1. Iso-probability contours for site removal, showing the influence of distance metrics and perimeter removal probability (q_p). The columns represent the square (L_∞), Euclidean (L_2), and Manhattan (L_1) distance metrics (**left** to **right**). The rows show decreasing probability q_p, with values $q_p = 0.75$ (**top**), $q_p = 0.50$ (**middle**), and $q_p = 0.275$ (**bottom**). The color scale indicates the local probability of a site remaining in the lattice, defined as $1 - q(d, q_p)$. Specifically, darker regions (near the edge) correspond to a higher probability of remaining ($1 - q \to 1$), while lighter regions (**center**) correspond to a higher probability of being removed ($q \to 1$). Here, q_p denotes the value of the removal probability exactly at the perimeter of the lattice.

The simulation proceeds as follows: Initially, a specific value for the boundary parameter q_p is assigned for the entire duration of the realization. In each step, a lattice location (i, j) is randomly chosen. If the site is already empty, a new location is chosen. If the site is occupied, its corresponding removal probability $q(i, j)$ is calculated based on its distance d from the center, using the fixed value of q_p in Equation (1). A uniformly distributed random number $R \in [0, 1]$ is generated and compared with the probability $q(i, j)$. If $R < q(i, j)$, the site is removed (becomes empty); otherwise, the site remains occupied. The process continues with the next randomly selected location. Following every successful site removal, the lattice is tested for the existence of the percolating cluster (spanning connectivity). This process continues until the red-bond point is found for the given realization.

In order to avoid checking to see if the spanning cluster has broken down after each site removal, which is very time-consuming, a two-stage method is used. First, a Coarse Search Phase is conducted where sites are removed in groups until non-percolation is detected. The Hoshen–Kopelman [1,2,4] algorithm is used effectively for fast cluster identification and percolation detection. Following the loss of spanning connectivity, a Fine Search Phase (Binary Search) is applied to the interval of the last removed sites. This binary approach precisely locates the minimum number of sites that must be restored (or, conversely, the maximum number that can be removed) to maintain connectivity, thus accurately defining

the critical threshold for the specific q_p and realization. To ensure statistical convergence and minimize fluctuations, we perform $N = 1000$ independent realizations for each set of parameters and average the resulting values. Exactly at the critical point, various quantities are calculated, such as the critical concentration $\langle p_c \rangle$, the size of the maximum cluster $\langle S_{\max} \rangle$, and various cluster moments, in order to fully characterize the percolation transition under the influence of the spatial probability gradient.

3. Results

We first vary the q_p value, and we calculate the value of the critical percolation threshold point. In Figure 2 we show schematics of typical realizations of the lattice for several different q_p values.

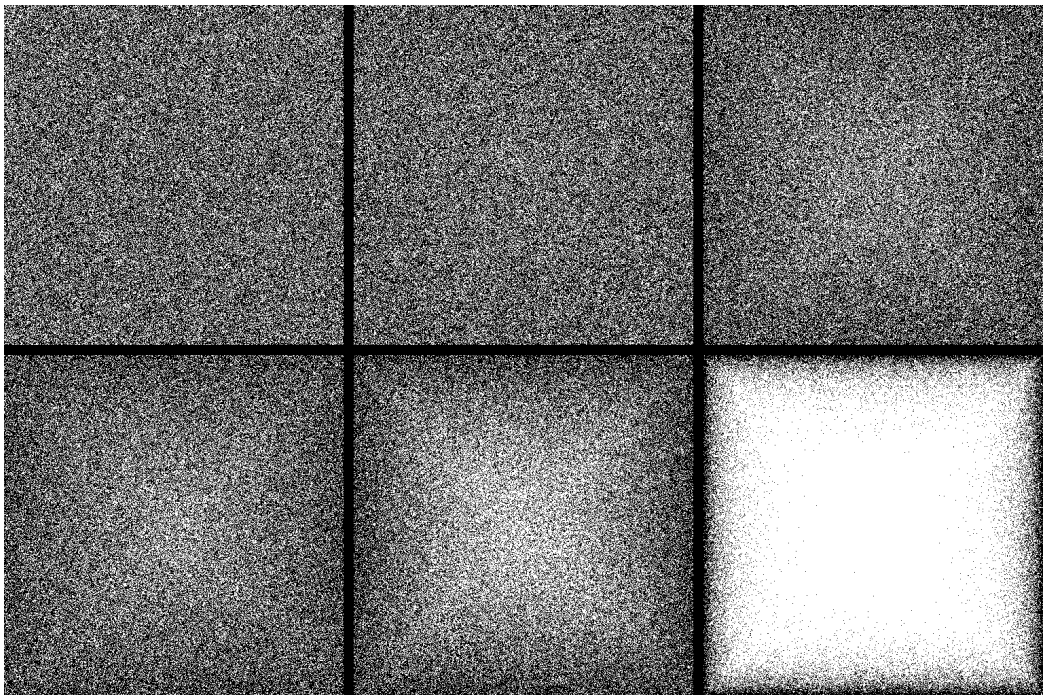

Figure 2. Site occupancy on an $L \times L$ square lattice at the critical probability $\langle p_c \rangle$ for different perimeter probabilities q_p ($q_p = 1, 0.8, 0.5, 0.4, 0.2, 0.01$). Unoccupied sites are shown in white, and occupied sites are shown in black. Note that for smaller q_p values, the higher density of black sites near the perimeter is consistent with the higher survival probability $(1 - q)$ shown in the darker regions of Figure 1.

The top-left panel of Figure 2, representing $q_p = 1$, corresponds to the classical percolation, which results in the well-known value of $p_c = 0.5927$. As q_p is reduced we see in the several plots of Figure 2 that the lattice starts to become empty in the middle, while the area close to the perimeter is still relatively more occupied, as is expected in this model. The corresponding spanning clusters for the same q_p values are given in Figure 3, where only the largest cluster is shown, verifying the results of the previous figure.

The actual value of p_c is plotted in Figure 4 as a function of q_p. Here we actually plot the value of $(1 - q_p)$, which corresponds to the non-removal probability, so that at the value $1 - q_p = 0$ we recover the p_c value of $p_c = 0.5927$. We observe a small decrease in the p_c value in the range up to $1 - q_p = 0.5$ and a much sharper decrease in the range 0.5–1.0 in a parabolic-like curve. This suggests that the presence of a highly protected perimeter ($q_p \to 0$) allows the percolating cluster to survive even at lower overall occupation probabilities. In the extreme case where $q_p = 1$, the removal probability $q(d, 1)$ becomes uniform throughout the entire lattice. Under this condition, the spatial gradient

vanishes, and every site is removed with certainty, leading to a completely vacant lattice. This represents the absolute upper bound of the infection process, where the system cannot sustain any connectivity. While we tried several fittings for the points of Figure 4, the reduction in p_c follows a non-linear trend that is accurately captured by a fourth-order polynomial fit, as detailed in Figure 4.

We next calculate the relative size of the largest connected cluster, $S_{\max}$ (normalized by the total number of sites), at the critical threshold p_c. Figure 5 illustrates that the maximum cluster size, $S_{\max}$, decreases linearly as a function of $(1 - q_p)$. The line has a negative slope (approximately -0.2), indicating a clear linear relationship. This linear dependence, described by the relation $S_{\max} \approx -0.20(1 - q_p)$, suggests that as the perimeter sites become less likely to be removed (higher $1 - q_p$), the relative size of the largest connected cluster at the critical point decreases. The spatial inhomogeneity forces the spanning cluster to highly constrained regions closer to the center ($q_p = 1$), effectively reducing the maximum cluster size that the lattice can support before fragmentation.

The total number of non-percolating clusters (normalized by the total number of sites), $n(p_c)/L^2$, was then calculated at the critical point p_c for each q_p value. Figure 6 shows that $n(p_c)$ increases as $(1 - q_p)$ increases, reaching a maximum near $(1 - q_p) \approx 0.9$, and then falls sharply at higher values. We observe a parabolic-like behavior for most of the $1 - q_p$ range. The subsequent sharp decrease is consistent with the rapid drop in p_c observed in Figure 4. The overall increase in the number of clusters indicates that the gradient in q promotes fragmentation and the creation of numerous small, isolated clusters at the critical point, especially when the perimeter is highly protected (low q_p).

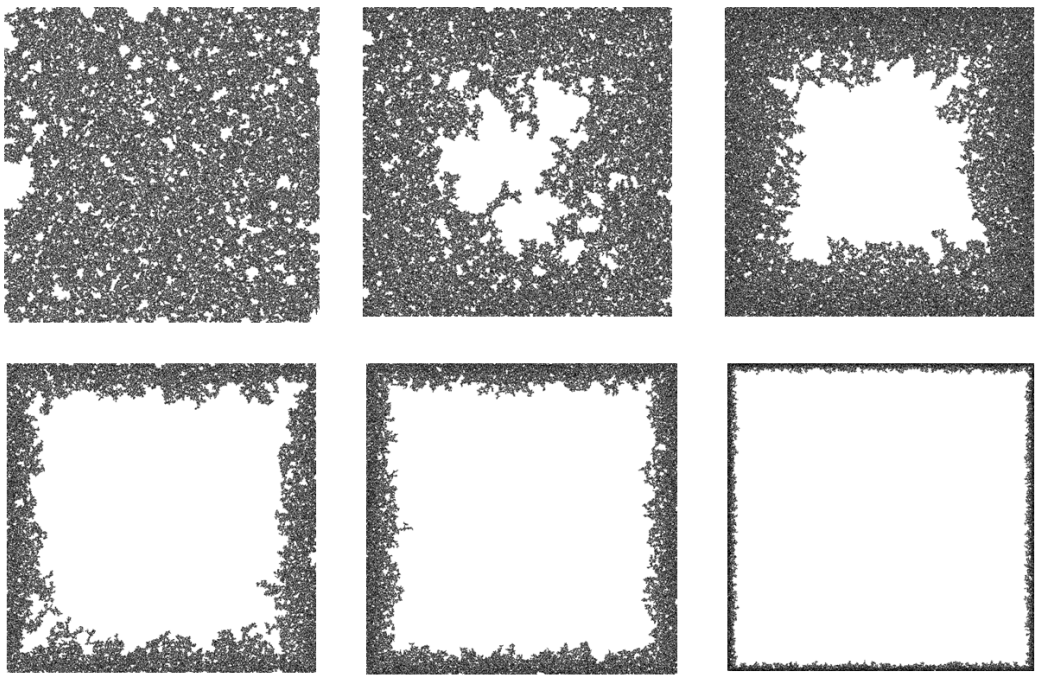

Figure 3. Giant cluster formed at $\langle p_c \rangle$ for the same cases as Figure 2. The black pixels represent the sites belonging to the spanning cluster. The concentration of the cluster toward the perimeter for decreasing q_p reflects the spatial gradient defined in Equation (1).

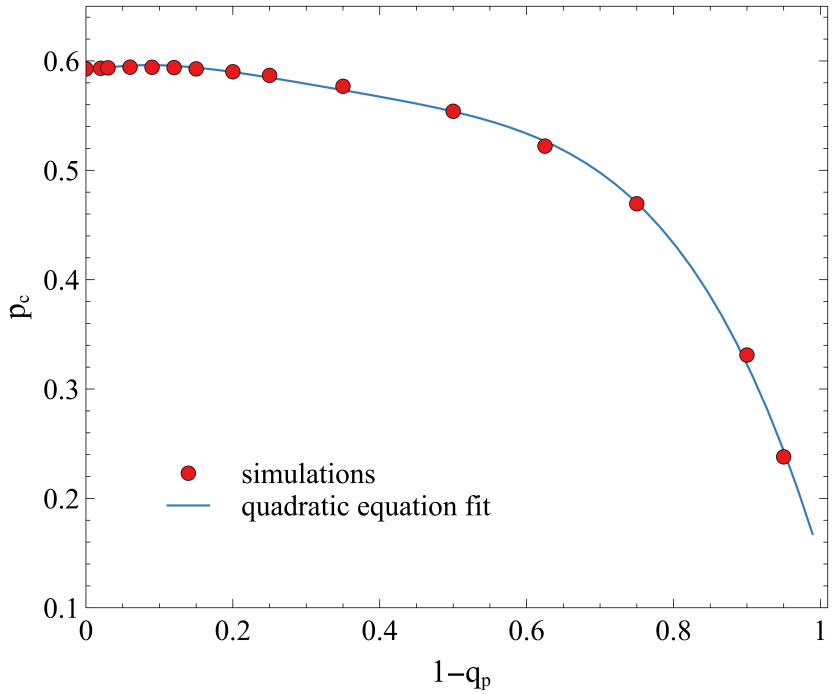

Figure 4. Dependence of the critical percolation threshold p_c on the perimeter parameter $(1 - q_p)$ for the case of the L_∞ metric. The solid line represents a fourth-order polynomial fit of the form $p_c(q_p) = \sum_{i=0}^{4} a_i(1 - q_p)^i$. The best-fit coefficients are determined as $a_4 = -1.7327$, $a_3 = 2.3102$, $a_2 = -1.1787$, $a_1 = 0.1555$, and $a_0 = 0.5902$. The reduced chi-square value ($\chi^2_{red} = 0.9707$) indicates an excellent agreement between the proposed model and the numerical data, supporting the geometric interpretation of the transition. Simulations were for lattice sizes $L = 1001$ and 1000 iterations.

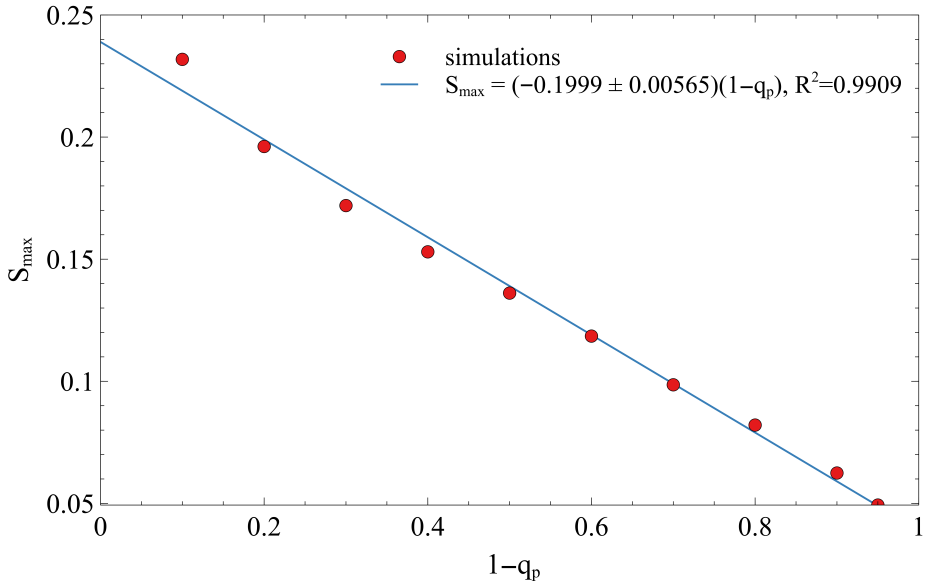

Figure 5. The variation in the maximum cluster size ($S_{\max}$) as a function of the non-removal probability at the perimeter $(1 - q_p)$ for a square lattice of size $L = 1001$. The relationship is linear $R^2 = 0.9909$, exhibiting a slope of approximately -0.2.

The distribution of cluster sizes, $N(s)$ (the number of clusters of size s), is crucial for characterizing the universality class of the transition, as it typically follows a power law: $N(s) \sim s^{-\tau}$. Figure 7 (in a log–log plot) confirms that the cluster size distribution follows a power law for all tested values of q_p. The calculated exponent, τ_{calc}, varies significantly with the parameter $1 - q_p$. For the classical 2D random percolation, the

exponent is $\tau = 187/91 \approx 2.055$. The inset of Figure 7 shows that τ_{calc} starts close to the theoretical value for $1 - q_p \to 0$, reaches a minimum near $1 - q_p \approx 0.5$, and then increases sharply for large $1 - q_p$, indicating a significant deviation from the classical percolation universality class due to the q-gradient. This suggests that the spatial inhomogeneity introduced by the gradient is strong enough to change the effective critical exponents, implying that the gradient percolation model may belong to a different universality class than random percolation.

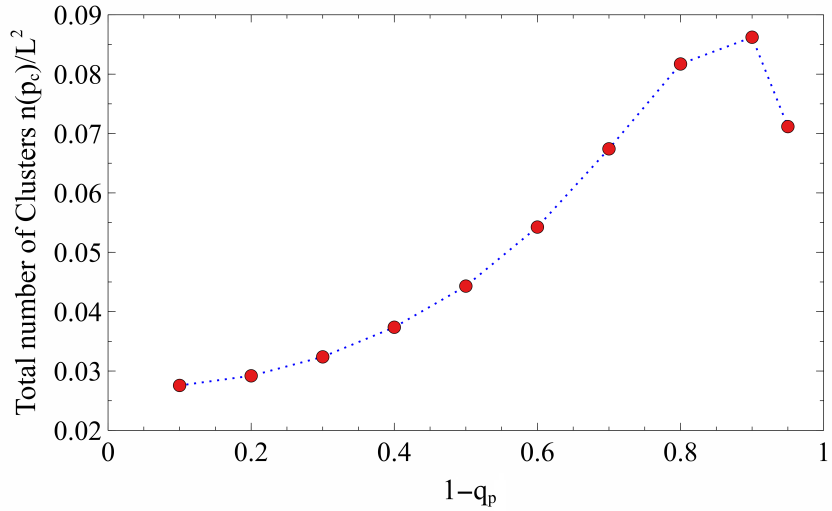

Figure 6. The behavior of the normalized mean number of total clusters, $n(p_c)/L^2$, at the critical point for various values of the perimeter non-removal probability $(1 - q_p)$ for a square lattice size of $L = 1001$. The mean total number of clusters exhibits a quadratic increase with respect to the perimeter non-removal probability $(1 - q_p)$.The red circles represent the simulation data, while the dashed blue line is added as optical guide.

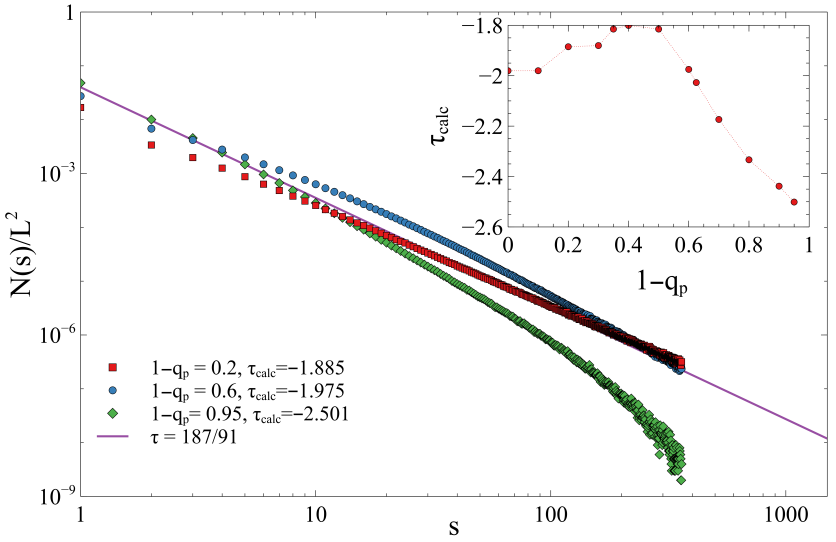

Figure 7. Normalized cluster size frequency distribution $(N(s)/L^2)$ versus the cluster size (s) on a log–log scale, examining the effect of the perimeter non-removal probability $(1 - q_p)$ on cluster statistics at the critical point. The inset shows the change in the slope τ_{calc} of the cluster size distributions with respect to $1 - q_p$. The red circles represent the simulation data, while the dashed line is added as optical guide.

4. Discussion and Conclusions

In the present work we introduced a percolation model with new rules for the occupancy of the sites. This research is motivated by the necessity to provide a quantitative framework to explain the concentrations of molecular ingredients in the vicinity of the tumor microenvironment. The binary nature of the percolation model could represent the existence or absence of key molecules as a function of the distance to the tumor cells. While the classical percolation model has been successful in the past in describing several realistic systems, in recent years several variations of the model have appeared in the literature, which may describe different applications. For example, see the Achlioptas model [38]. In all these variations the key characteristic is that the critical parameter values vary significantly from the classical model. This may lead one to prepare a system that exhibits a desired critical threshold value [39]. In the present case we show how the depletion zone around the center of the lattice strongly affects the creation of the spanning cluster, reducing the critical threshold to a very low value. This reduction was shown to follow a parabolic behavior. The parameter q_p serves to regulate the spatial gradient of the removal probability between the lattice center and the perimeter, thereby controlling the boundary conditions of the infection process. We find that the size of the maxi-cluster falls linearly with $1 - q_p$ with a slope of ≈ -0.20. Our results may be useful in explaining the behavior of the tumor microenvironment, and subsequently the control of the efficiency of possible therapies, in an effort to find the optimal amount of radiation and chemotherapy tailored for each individual case.

The proposed model's ability to simulate spatial gradients via the parameter q_p aligns with established findings on the heterogeneity of the tumor microenvironment (TME) [25,40]. Such gradients are known to impede the delivery of therapeutic agents and oxygen, particularly in hypoxic regions [41,42], which can now be quantitatively analyzed through the lens of distance-dependent percolation.

Author Contributions: Conceptualization, P.A.; data curation, E.L.; formal analysis, E.L. and P.A.; funding acquisition, P.A.; investigation, E.L.; methodology, E.L. and P.A.; project administration, P.A.; resources, E.L.; software, E.L.; supervision, P.A.; visualization, P.A.; writing—original draft, E.L. and P.A.; writing—review and editing, E.L. and P.A. All authors have read and agreed to the published version of the manuscript.

Funding: P.A. acknowledges the University of Thessaloniki Project No. 85106 for partial funding support.

Data Availability Statement: The data and code that support the findings of this study are openly available in GitHub at https://github.com/lef27064/PercWithDistDepData, accessed on 18 December 2025.

Conflicts of Interest: The authors declare no conflict of interest. The funders had no role in the design of the study; in the collection, analyses, or interpretation of data; in the writing of the manuscript; or in the decision to publish the results.

References

1. Stauffer, D.; Aharony, A. *Introduction to Percolation Theory*, 2nd ed.; Taylor & Francis: Abingdon-on-Thames, UK, 1994.
2. Gould, H.; Tobochnik, J.; Christian, W. *An Introduction to Computer Simulation Methods*; Addison-Wesley: Boston, MA, USA, 2006.
3. Kirkpatrick, S. Percolation and Conduction. *Rev. Mod. Phys.* **1973**, *45*, 574. [CrossRef]
4. Hoshen, J.; Kopelman, R. Exciton Percolation I. Migration Dynamics. *J. Chem. Phys.* **1976**, *65*, 2817–2823. [CrossRef]
5. Larson, R.G.; Scriven, L.E.; Davis, H.T. Percolation Theory of Two Phase Flow in Porous Media. *Chem. Eng. Sci.* **1981**, *36*, 57–73. [CrossRef]
6. Katz, A.J.; Thompson, A.H. Quantitative Prediction of Permeability in Porous Media. *Phys. Rev. B* **1986**, *34*, 8179. [CrossRef]
7. Coniglio, A.; Stanley, H.E.; Klein, W. Percolation and the Elasticity of Gels. *Phys. Rev. Lett.* **1979**, *42*, 518–521. [CrossRef]

8. Beech, H.K.; Lin, T.S.; Sen, D.; Rota, D.; Olsen, B.D. Kinetics of Polymer Gel Formation Cause Deviation from Percolation Theory in the Dilute Regime. *Macromolecules* **2023**, *56*, 9255–9263. [CrossRef]
9. Söllner, J.; Neimark, A.V.; Thommes, M. Development and Application of an Advanced Percolation Model for Pore Network Characterization by Physical Adsorption. *Langmuir* **2024**, *40*, 17092–17105. [CrossRef]
10. Wang, J.; Wang, S.; Li, H. Sorption–Deformation–Percolation Model for Diffusion in Nanoporous Media. *ACS Nano* **2023**, *17*, 3698–3707.
11. Dorogovtsev, S.N.; Goltsev, A.V.; Mendes, J.F.F. Percolation and Localization in Complex Networks. *Phys. Rev. E* **2001**, *64*, 046104.
12. Cohen, R.; ben Avraham, D.; Havlin, S. Percolation Critical Exponents in Scale-Free Networks. *Phys. Rev. E* **2002**, *66*, 036113. [CrossRef] [PubMed]
13. Albert, R.; Jeong, H.; Barabási, A.L. Error and Attack Tolerance of Complex Networks. *Nature* **2000**, *406*, 378–382. [CrossRef]
14. Buldyrev, S.V.; Parshani, R.; Paul, G.; Stanley, H.E.; Havlin, S. Catastrophic Cascade of Failures in Interdependent Networks. *Nature* **2010**, *464*, 1025–1028. [CrossRef]
15. Newman, M.E.J. Spread of Epidemic Disease on Networks. *Phys. Rev. E* **2002**, *66*, 016128. [CrossRef] [PubMed]
16. Gallos, L.K.; Cohen, R.; Argyrakis, P.; Bunde, A.; Havlin, S. Stability and Topology of Scale-Free Networks Under Attack and Defense Strategies. *Phys. Rev. Lett.* **2005**, *94*, 188701. [CrossRef]
17. Daley, D.J.; Kendall, D.G. Epidemics and Rumours. *Nature* **1964**, *204*, 1115. [CrossRef] [PubMed]
18. Valdivino, V., Jr.; Machado, F.P.; Ravishankar, K. The Rumor Percolation Model and Its Variations. *arXiv* **2016**, arXiv:1612.03853. [CrossRef]
19. Bhansali, R.; Schaposnik, L.P. A Trust Model for Spreading Gossip in Social Networks: A Multi-Type Bootstrap Percolation Model. *Proc. R. Soc. A Math. Phys. Eng. Sci.* **2020**, *476*, 20190826. [CrossRef]
20. Centola, D. The Spread of Behavior in an Online Social Network Experiment. *Science* **2010**, *329*, 1194–1197. [CrossRef] [PubMed]
21. Chen, S.; Liu, C.; Li, C. Indirect Influence in Social Networks as an Induced Percolation Phenomenon. *Proc. Natl. Acad. Sci. USA* **2022**, *119*, e2100151119.
22. Garas, A.; Argyrakis, P.; Rozenblat, C.; Tomassini, M.; Havlin, S. Worldwide Spreading of Economic Crisis. *New J. Phys.* **2010**, *12*, 113043. [CrossRef]
23. Dimou, A.; Argyrakis, P.; Kopelman, R. Tumor Biochemical Heterogeneity and Cancer-Radiochemotherapy: Network Breakdown Zone-Model. *Entropy* **2022**, *24*, 1069. [CrossRef]
24. Dimou, A.; Argyrakis, P.; Kopelman, R. Tumor Hypoxia Heterogeneity Affects Radiotherapy: Inverse Percolation Shell Model Monte Carlo Simulations. *Entropy* **2022**, *24*, 86. [CrossRef]
25. Vaupel, P.; Harrison, L. Tumor Hypoxia: Causative Factors, Compensatory Mechanisms, and Cellular Response. *Oncologist* **2004**, *9*, 4–9. [CrossRef]
26. Brown, J.M.; Wilson, W.R. Exploiting Tumour Hypoxia in Cancer Treatment. *Nat. Rev. Cancer* **2004**, *4*, 437–447. [CrossRef]
27. Eil, R.; Vodnala, S.K.; Clever, D.; Klebanoff, C.A.; Sukumar, M.; Pan, J.H.; Restifo, N.P. Ionic Immune Suppression Within the Tumour Microenvironment Limits T Cell Effector Function. *Nature* **2016**, *537*, 539–543. [CrossRef]
28. Singleton, D.C.; Macann, A.; Wilson, W.R. Therapeutic Targeting of the Hypoxic Tumour Microenvironment. *Nat. Rev. Clin. Oncol.* **2021**, *18*, 751–772. [CrossRef]
29. Noman, M.Z.; Hasmim, M.; Messai, Y.; Terry, S.; Kieda, C.; Janji, B.; Chouaib, S. Hypoxia: A Key Player in Antitumor Immune Response. *Am. J. Physiol. Cell Physiol.* **2015**, *309*, C487–C499. [CrossRef] [PubMed]
30. Chen, B.; Song, Y.; Zhu, X.; Xu, Z. PKM2, the "K^+ Sink"in the Tumor Interstitial Fluid. *Front. Cell Dev. Biol.* **2022**, *10*, 1070802.
31. Lee, C.; Folz, J.; Tan, J.; Jo, J.; Wang, X.; Kopelman, R. Chemical Imaging In-Vivo: Photoacoustics Based 4-Dimensional Chemical Analysis. *Anal. Chem.* **2019**, *91*, 2561–2569. [CrossRef]
32. Warburg, O. On the Origin of Cancer Cells. *Science* **1956**, *123*, 309–314. [CrossRef] [PubMed]
33. Tannock, I.F.; Rotin, D. Acid pH in Tumors and Its Potential for Therapeutic Exploitation. *Cancer Res.* **1989**, *49*, 4373–4384.
34. Vaupel, P.; Kallinowski, F.; Okunieff, P. pHe and Its Biological Importance in Cancer Tissue. *Cancer Res.* **1989**, *49*, 6449–6465.
35. Fu, J.; Wu, Q.; Dang, Y.; Lei, X.; Feng, G.; Chen, M.; Yu, X. Synergistic Therapy Using Doxorubicin-Loading and Nitric Oxide-Generating Hollow Prussian Blue Nanoparticles with Photoacoustic Imaging Potential Against Breast Cancer. *Int. J. Nanomed.* **2021**, *16*, 6003–6016. [CrossRef]
36. Stanley, H.E. *Introduction to Phase Transitions and Critical Phenomena*; Oxford University Press: Oxford, UK, 1971.
37. de Berg, M.; Cheong, O.; van Kreveld, M.; Overmars, M. *Computational Geometry: Algorithms and Applications*, 3rd ed.; Springer: Berlin/Heidelberg, Germany, 2008.
38. Achlioptas, D.; D'Souza, R.; Spencer, J. Explosive Percolation in Random Networks. *Science* **2009**, *323*, 1453. [CrossRef]
39. Giazitzidis, P.; Avramov, I.; Argyrakis, P. Variation of the critical percolation threshold with the method of preparation of the system. *Eur. Phys. J. B* **2015**, *88*, 331. [CrossRef]
40. Baish, J.W.; Jain, R.K. Fractals and cancer. *Cancer Res.* **2000**, *60*, 3683–3688.

41. Jain, R.K. Transport of molecules in the tumor interstitium: A review. *Cancer Res.* **1987**, *47*, 3039–3051. [PubMed]
42. Toma-Dasu, I.; Dasu, A. Hypoxia—A continuous challenge for radiobiology. *AIP Conf. Proc.* **2013**, *1530*, 101–108.